Photo induced absorption study of model organic charge transfer systems
by Amy Alta Elizabeth Hyfield

A thesis submitted in partial fulfillment of the requirements for the degree of Master of Science in Chemistry
Montana State University

Abstract:
The wide use of lasers and their potential as a harmful device has created a need for ways to intelligently block these intense light sources called optical limiters. Reverse Saturable Absorption (RSA) has been targeted as a type of non-linear process that can result' in optical limiting. This research focuses on achieving RSA through the formation of transient charged species such as polarons and bipolarons via photo induced charge transfer. In order to effectively engineer materials for this application, it is important to gain an understanding about the structure-property relationships that exist among the molecular systems as well as the processes occurring after photoexcitation. This thesis examines the general trends of the rate constants for diffusion limited forward and reverse electron transfer of novel organic donor molecules in solution with C60, a known electron acceptor. It also looks at the quantum efficiency of the formation of solvated ions calculated via their maximum absorbance and through a new method of determination involving an isobestic point. The quantum yield efficiency of C60 triplet quenching is also calculated and an attempt to reconcile the difference between this yield and the yield of solvated ions is presented.

/

PHOTO INDUCED ABSORPTION STUDY OF MODEL ORGANIC CHARGE TRANSFER SYSTEMS

by

Amy Alta Elizabeth Hyfield

A thesis submitted in partial fulfillment
of the requirements for the degree

of

Master of Science

in

Chemistry

MONTANA STATE UNIVERSITY
Bozeman, Montana

July 2000

APPROVAL

of a thesis submitted by

Amy Hyfield

This thesis has been read by each member of the thesis committee and has been found to be satisfactory regarding content, English usage, format, citations, bibliographic style, and consistency, and is ready for submission to the College of Graduate Studies.

Dr. Lee Spangler ______ Lee H. Spangler ______ 7-20-2000
(Signature) (Date)

Approved for the Department of Chemistry

Dr. Paul Grieco ______ Paul A. Grieco ______ 7-20-00
(Signature) (Date)

Approved for the College of Graduate Studies

Dr. Bruce McLeod ______ Bruce R. McLeod ______ 7-21-00
(Signature) (Date)

STATEMENT OF PERMISSION TO USE

Signature ____________________

Date 07·19·00

ACKNOWLEDGMENTS

I would like to thank Dr. Lee Spangler for his mentorship through my years at Montana State University. His knowledge, creativity and understanding are unparalleled. I would also like to thank the countless souls in the Department of Chemistry, the Department of Physics and throughout the University for their guidance and friendship. This includes, most especially: Dr. Charles Spangler and the C. Spangler group; the people of Scientific Materials Corporation; Dr. Pat Callis; Dr. David Singel; Mary McLaughlin and my lab mates, especially Wendi Sonnenberg, Yanong Han, Jeff Wilcox, Tony Smith, Hu Li and Tami Faircloth. As life requires balance, I must also thank my dear cycling buddies, who helped me maintain my sanity and perspective and my family, especially Milo, who have always supported me and my wild dreams.

I would also like to express my gratitude to the Montana Space Grant Consortium, which funded a large portion of this research though a Graduate Fellowship for the academic year 1999-2000. Additional funding for this project comes from the AFOSR, BMDO, ARO and Scientific Materials Corporation, Bozeman, MT.

TABLE OF CONTENTS

TABLE OF CONTENTS – CONTINUED

LIST OF TABLES

LIST OF FIGURES

LIST OF FIGURES - CONTINUED

LIST OF FIGURES – CONTINUED

LIST OF SCHEMES

ACRONYMS

A	Acceptor
D	Donor
FTIR	Fourier Transform Infrared Spectroscopy
FTS	Fourier Transform Spectroscopy
FTVIS	Fourier Transform Visible Spectroscopy
HeNe	Helium Neon laser
IADC	Internal Analog to Digital Converter
Kn1	Hydroxy substituted Diphenylamino diphenylpolyene with one double bond
Kn2	Hydroxy substituted Diphenylamino diphenylpolyene with two double bonds
Kn3	Hydroxy substituted Diphenylamino diphenylpolyene with three double bonds
n=1	Bis-(diphenylamino) diphenylpolyene with one double bond
n=2	Bis-(diphenylamino) diphenylpolyene with two double bonds
n=3	Bis-(diphenylamino) diphenylpolyene with three double bonds
OD	Optical Density
ODCB	o-dichlorobenzene
PIA	Photo Induced Absorption
PI-CT	Photo Induced Charge Transfer
RSA	Reverse Saturable Absorption

ABSTRACT

The wide use of lasers and their potential as a harmful device has created a need for ways to intelligently block these intense light sources called optical limiters. Reverse Saturable Absorption (RSA) has been targeted as a type of non-linear process that can result in optical limiting. This research focuses on achieving RSA through the formation of transient charged species such as polarons and bipolarons via photo induced charge transfer. In order to effectively engineer materials for this application, it is important to gain an understanding about the structure-property relationships that exist among the molecular systems as well as the processes occurring after photoexcitation. This thesis examines the general trends of the rate constants for diffusion limited forward and reverse electron transfer of novel organic donor molecules in solution with C_{60}, a known electron acceptor. It also looks at the quantum efficiency of the formation of solvated ions calculated via their maximum absorbance and through a new method of determination involving an isobestic point. The quantum yield efficiency of C_{60} triplet quenching is also calculated and an attempt to reconcile the difference between this yield and the yield of solvated ions is presented.

CHAPTER 1

INTRODUCTION

Optical Limiting

The introduction of the laser has revolutionized optical science and everyday life as well. Along with its beneficial applications in areas like medicine and research, come its unfortunate dangers. Lasers can be a high powered and destructive tool with the capability to easily blind or destroy optically sensitive materials such as detectors or eyes. Therefore, important research is being performed with the goal of developing more intelligent ways to block high-powered light sources.

Filters are currently the primary method used to attenuate lasers. They have the undesirable effect, however, of completely stopping all of the light at the wavelengths over which they are designed to protect, regardless of the light's intensity. The result is that a person or detector can not see these colors at all which can be inconvenient and dangerous. With the development of lasers in wavelengths ranging from the UV to the IR, protecting a device against a strike from the myriad of possibly damaging sources through the use of filters would render the device useless. This is why the development of a "smart" filter that is active over a broad wavelength range, known as an optical limiter, is necessary. An ideal optical limiter must fulfill several demands. It must be a passive device; that is, the light that it is designed to protect against should activate the limiting mechanism. It should be transmissive to low levels of light, such as room light, but opaque at higher intensity levels. It should limit over a wide wavelength range and it should work on time scales as short as hundreds of femtoseconds as well as protect against CW sources. It should not damage easily and should be able to block multiple pulses. All of these demands do not necessarily need to be the burden of one compound. Several different materials, both organic and inorganic, can be used in tandem to bring about the desired effect.

Optical Limiting Mechanism

Many different mechanisms have been proposed to bring about optical limiting. The focus in this research is on Reverse Saturable Absorption (RSA). In this mechanism (see Figure 1), weak ground state absorption populates the first excited state of a molecule. At low light levels, few molecules absorb and therefore there is minimal population in this state. This being the case, other absorption pathways play a negligible part in the attenuation and the over all absorption of the molecule is linear. When the population in this excited state becomes appreciable, as in the case with an incident laser beam, other processes begin to play a role. From this excited state, the molecule can yield several different transient species that can have subsequent absorption. When these additional absorption processes "turn on" the result is non-linear absorption where one molecule absorbs two or more photons before relaxing back to its ground state. If the higher level absorptions by these transient species are resonant with the ground state absorption, then optical limiting is the result.

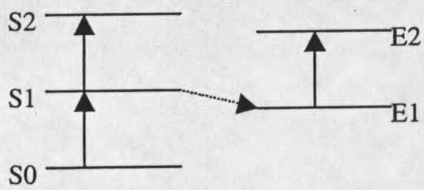

Figure 1. Reverse Saturable Absorption. S0 is the ground state, S1 is the first excited state, S2 is an additional excited state of the same molecule, E1 and E2 represent excited states of a different species

The nature of the transient depends on the compound being used. The transient can be either an excited singlet or triplet state. It could be an excited state of another molecule populated in energy transfer, or it could be an ionic state of either the photo-prepared molecule or another molecule generated by electron transfer. In any case, the transient species must be created quickly, efficiently and it should have a very strong absorption in order to optimize the RSA process.

Photo-induced Charge Transfer

The compounds under investigation in this study are known to form highly absorbing charged states when chemically oxidized. These cationic (polaron) and di-cationic (bipolaron) species are fairly stable and tunable over a wide range of wavelengths extending from ~ 500nm to ~1000nm depending on the conjugation length in the molecule. These molecules could potentially be used for limiting if the absorption of the charged and neutral species sufficiently overlap and if the charged species can be photo-induced.

Photo-induced charge transfer has been seen in many different compounds, for instance, it is the initial step in photosynthesis. Two simple models have been proposed by Sariciftci and Heeger[1] to explain basic photo-induced charge transfer: electron transfer and hole transfer (see Figure 2). In electron transfer the donor molecule is prepared in an excited state by the absorption of a photon. The electron is then transferred to the LUMO of a nearby acceptor molecule. A cation and an anion result, each with new absorption capabilities. In hole transfer, the incoming light excites the acceptor. An electron from the HOMO of the donor molecule moves to the now vacant position in the HOMO of the acceptor, again yielding a cation and an anion.

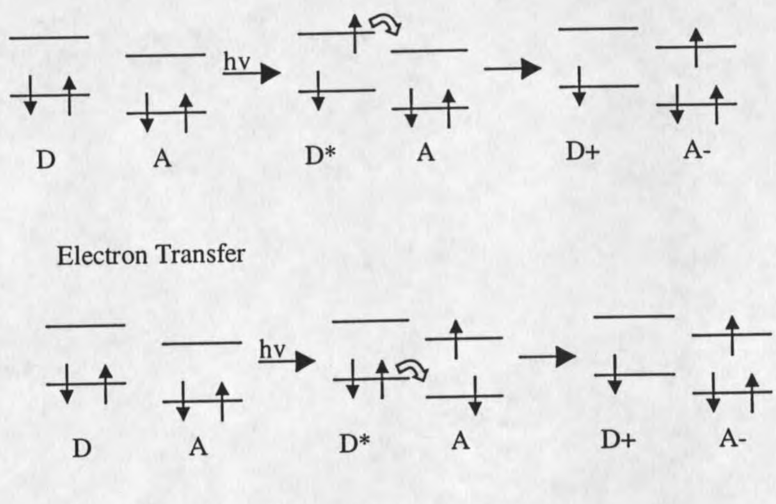

Figure 2. Electron and Hole Transfer. Charge can be transferred to create ions from neutral molecules through the transfer of an electron, top, or a hole, bottom. D is the donor molecule and A is the acceptor molecule.

Classical Charge Transfer Theory[2]

It is important to understand the process of electron transfer in order that the efficiency and rate with which ions are formed can be maximized. Much of the electron transfer theory today centers on the ideas of R.A. Marcus [2,3], who sought to describe outer-sphere electron transfer in ground state species, as well as additional work by Hush[2,4] and Rehm and Weller[5]. The ideas are easily applied to molecules in the excited state. The general mechanism for charge transfer goes as follows[2]:

$$D + A \underset{k_d}{\overset{k_a}{\rightleftarrows}} D|A$$

$$D|A \underset{k_{-ET}}{\overset{k_{ET}}{\rightleftarrows}} D^+|A^-$$

$$D^+|A^- \xrightarrow{k_{sol}} D^+ + A^-$$

Scheme 1. Mechanism for Charge Transfer. D is the donor molecule, A is the acceptor molecule, D | A represents a donor/acceptor complex

In the first step, the donor and acceptor molecule diffuse together to form a precursor complex D | A. This process is controlled by two rate constants, k_a and k_d, the rate of association and dissociation, respectively. k_a usually approaches the diffusion-controlled limit, on the order of 6 x 10^9 liters/mole-sec for neutral molecules in water[6]. In the second step, the precursor complex moves toward a transition state in which electron transfer takes place to form a successor complex, $D^+|A^-$. The movement toward a transition state involves solvent reorganization to account for the movement of the electron in the electron transfer step. In addition, due to the Franck-Condon principle, the nuclear configuration of the precursor and successor complexes at this transition state needs to be the same.

The kinetics of the electron transfer is a key parameter in the understanding of this process. The rate constants embody such elements as the potential energy of the different states, the reorganization energy, as well as the nature of the characters. The rate of electron transfer can be written as:

$$k_{ET} = \kappa_{el}\upsilon_n \exp\left[-\frac{(\lambda + \Delta G^0)^2}{4\lambda k_B T}\right] \qquad 1$$

Where k_{ET} is the rate constant of electron transfer, κ_{el} is the electronic transmission coefficient, usually taken to be 1, υ_n is the nuclear motion through the transition state ($\upsilon_n \sim 10^{13}$ s^{-1}), ΔG^0 is the Gibbs free energy, k_B is the Boltzman constant, T is the temperature and λ is the reorganization energy. Two of the most important parameters in this equation are the reorganization energy and the Gibbs free energy and so a brief examination of their components is useful.

ΔG^0 between the reactant state, D + A, and the product state, $D^+ + A^-$, is given by the following expression:

$$\Delta G^0 = e\left(E^0_{D+/D} - E^0_{A/A-}\right) + \omega^P - \omega^R \qquad 2$$

where e is the charge of an electron, $E^0_{D+/D}$ and $E^0_{A/A-}$ are the standard reduction potentials for D^+ and A^- and ω^P and ω^R correct for the work done when bringing D^+ and

A^- and D and A together, respectively and are usually negative. It is thus clear that the Gibbs free energy is smaller when the reduction potentials of the ionic species generated are similar. The electron transfer reaction can be visualized as intersecting Gibbs free energy curves when plotted along the reaction coordinate. These are approximated by parabolas and, according to Marcus theory, the curvature of the reactant and product curves are assumed to be the same. Figure 3 shows these curves under varying conditions.

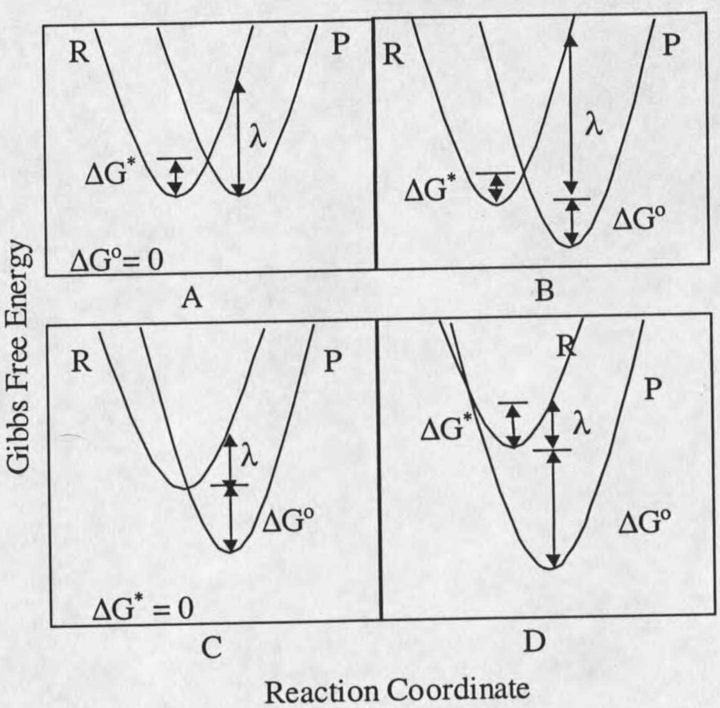

Figure 3. Diagrams Showing the Intersection of the Gibbs Energy Surfaces for the Reactant (R) State (D | A) and the Product (P) State (D^+ | A^-). (a) an isoergonic reaction with $\Delta G^0=0$; (b) the normal region where $0\leq -\Delta G^0 \geq \lambda$ (c) the condition for maximum rate constant where $-\Delta G^0=\lambda$; (d) the "inverted region" where $-\Delta G^0 > \lambda$.[2]

Here we see the reorganization energy is defined as the change in the Gibbs free energy if the reactant state were to distort to the product state without the transfer of an electron. ΔG^* is the Gibbs energy of activation for the electron transfer reaction and ΔG^0 is the difference between the Gibbs energy of the reactant and product states when the donor and acceptor are a distance r_{DA} apart. ΔG^* is defined as

$$\Delta G^* = \frac{(\lambda + \Delta G^0)^2}{4\lambda} \qquad 3$$

Clearly, based on equations 1 and 3 and figure 3, the rate of electron transfer will increase and the activation energy will decrease as ΔG^0 becomes more negative, until the maximum rate is obtained at $-\Delta G^0 = \lambda$. If ΔG^0 becomes increasingly more negative, the rate is predicted to decrease again. This is known as the Marcus "inverted region". The second important parameter in the rate equation is the reorganization energy, λ. This is usually made up of two contributing factors: the solvent- independent term, λ_{in} and the solvent-dependant term, λ_{out} , so that,

$$\lambda = \lambda_{in} + \lambda_{out} \qquad 4$$

λ_{in} is due to structural differences in the reactant and product equilibrium states. This is usually treated harmonically,

$$\lambda_{in} = \frac{1}{2}\sum_i \bar{f}_i \left(r_R^{eq} - r_P^{eq}\right)^2 \qquad 5$$

where r_R^{eq} and r_P^{eq} are the equilibrium bond lengths in the reactant and product states, respectively, $\bar{f}_i$ is the reduced force constant for the ith vibration and the sum is taken over all relevant intramolecular vibrations. λ_{out} is called the solvent reorganization energy as it is due to the changes in orientation and polarization of the solvent induced by the transition from D|A to D^+| A^-. In order to calculate this value, the solvent is treated as a dielectric continuum,

$$\lambda_{out} = \frac{1}{2}\varepsilon_0\left[\frac{1}{\varepsilon_{op}} - \frac{1}{\varepsilon_s}\right]\int\left(E^R - E^P\right)^2 dV \qquad 6$$

E^R and E^P are the electric field exerted in vacuum at a distance r from the centers of the reactant and product states, ε_{op} and ε_s are the optical and static dielectric constants of the solvent ($\varepsilon_{op} = n^2$ where n is the refractive index of the medium), and ε_0 is the permittivity of vacuum. A spherical reagent model is assumed so that the appropriate boundary conditions may be set for the integration, which is carried out over the volume. Ellipsoidal models have also been considered, but this generates more complex equations for λ_{out}. Therefore the equation after the integration is,

$$\lambda_{out} = \frac{(\Delta e)^2}{4\pi\varepsilon_0}\left[\frac{1}{2a_D} + \frac{1}{2a_A} - \frac{1}{r_{DA}}\right]\left[\frac{1}{\varepsilon_{op}} - \frac{1}{\varepsilon_s}\right] \qquad 7$$

Where Δe is the charge transferred, a_D and a_A are the atomic radii of the donor and acceptor and r_{DA} is the center to center distance between the donor and acceptor. In very non-polar solvents, $\varepsilon_{op} \approx \varepsilon_s$ and λ_{out} is very nearly zero. For very polar solvents, the solvent reorganization energy can be as much as 1.0-1.5 eV and becomes the dominating term in the total reorganization energy, λ. As stated before, the rate, k_{ET} reaches its maximum value when $-\Delta G^0 = \lambda$. Therefore, we can assume that a smaller λ means that the maximum rate can be achieved without having to have a more exergonic reaction.

However, non-polar solvents have other less desirable qualities, especially when one considers the entire electron transfer mechanism's efficiency, including back electron transfer and solvation of ions.

One of the assumptions made in this analysis is that κ_{el}, the electronic transmission coefficient, is equal to unity. This assumption implies that the reaction is adiabatic and there is a unit probability of electron transfer at the transition state. The electronic coupling energy, H_{rp}, is moderately large in this case and there is significant overlap between the equilibrium wave functions of the reactant and product states. Adiabatic charge transfer occurs when the donor and acceptor molecules are in close proximity (van der Waals contact or close intramolecular proximity) because H_{rp} falls off exponentially with distance. However, electron transfer can occur in cases where there is little electronic coupling, H_{rp} is small and $\kappa_{el} \ll 1$. This is non-adiabatic electron transfer and it can occur through three pathways. The first occurs when the nuclear configuration of the reactant and the product states are equivalent at the transition state and H_{rp} is small. The electron is transferred through electronic tunneling at the transition state (see Figure 4). The overall reaction rate is temperature dependant because of the extra energy needed to reach the intersection point. Secondly, the system can undergo activated nuclear tunneling. This occurs where the R and P surfaces are close enough for a thermally activated electron to tunnel from the reactant to the product state. It occurs at an activation energy below that of the intersection point (see wave function b of Figure 4) however, this method is still temperature dependent. The third type of non-adiabatic charge transfer is temperature-independent nuclear tunneling. This tunneling occurs from the ground state of the reactant to the product state. It is not usually a very favorable transfer process and is illustrated by wave function c of Figure 4.

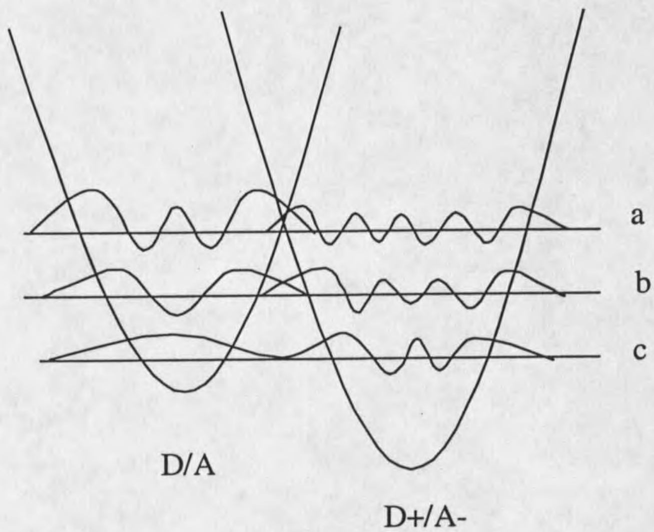

Figure 4. Potential Energy Diagram for the Quantum Mechanical Model of Electron Transfer. The vibrational wave functions are shown symbolically to illustrate tunneling. D/A and D+/A- indicate the reactant and product states respectively. Wave function a illustrates electron tunneling at the activation barrier, wave function b illustrates activated nuclear tunneling and wave function c shows temperature-independent nuclear tunneling.

The rate constant is dictated by Fermi's Golden Rule, that is, it is dictated by the square of the electronic interaction and the density of states. The quantum mechanical treatment of the electron transfer rate eventually coincides with the classical treatment (equation 1) as provided in the adiabatic case.

$$\mathrm{k_{ET}} = \frac{2\pi}{\hbar} H_{rp}^2 \left(4\pi\lambda k_B T\right)^{\frac{-1}{2}} \exp\left[-\frac{\left(\lambda + \Delta G^0\right)^2}{4\lambda k_B T}\right] \qquad 8$$

Provided that

$$K_{el}V_n = \frac{2\pi}{\hbar} H_{rp}^2 \left(4\pi\lambda k_B T\right)^{\frac{-1}{2}} \qquad 9$$

Clearly a compromise between solvent reorganization and Gibbs free energy exists that maximizes the electron transfer rate for the system. The difficulty is finding it for each particular system.

In many cases, especially in systems dealing with low concentrations in solution, the electron transfer rate is not the limiting rate, nor is it the only thing affecting the efficiency of the conversion. For instance, many electron transfer reactions in solution are diffusion limited.

Diffusion Limited Reactions[6]

The process of diffusion is fairly well understood and has been modeled for many different systems. The general phenomenological rate constant of a bimolecular reaction in solution is given by the following equation:

$$k = \frac{4\pi\left(D_A + D_B\right)\beta}{1 + \left[4\pi\left(D_A + D_B\right)\beta / k_R \exp\left\{-V(R)/k_B T\right\}\right]} \qquad 10$$

In this equation, D_A and D_B are the diffusion coefficients for molecules A and B respectively, β is calculated in the following way:

$$\beta^{-1} \equiv \int_R^{\infty} \frac{\exp(V(r)/k_B T)}{r^2} dr \qquad 11$$

V(r) is the potential energy, defined as:

$$V(r) = \frac{z_A z_B e^2}{\varepsilon r} \qquad 12$$

Where ε is the dielectric constant, z_A and z_B are the charges on molecules A and B respectively and e is the charge of an electron.

A diffusion limited reaction occurs when each encounter between the two molecules, A and B, results in a reaction. In this case, the rate constant for the reaction, k_R , is very large and the denominator for equation 10 becomes 1. If neutral molecules are considered, β = R and the diffusion limited rate constant becomes:

$$k_D = 4\pi(D_A + D_B)R \qquad 13$$

where R is the contact radius, $r_A + r_B$. The above equations were derived using a simple model that assumes spherical isotropic particles. The diffusion coefficient, D, is related to the viscosity of the solvent via the Einstein-Stokes relationship:

$$D = \frac{k_B T}{6\pi r \eta(T)} \qquad 14$$

Where η(T) is the temperature dependent viscosity of the solvent, r is the radius of the particle, k_B is the Boltzman constant and T is absolute temperature. The rate constant then becomes,

$$k_D = \frac{2k_B T(r_A + r_B)^2}{3\eta(T) r_A r_B} \qquad 15$$

In reactions involving ions, as in the recombination of the cationic and anionic species generated in photo-induced charge transfer, the potential energy term is no longer zero. β then becomes,

$$\beta = \frac{-z_A z_B r_0}{1-\exp(z_A z_B r_0 / R)} \qquad 16$$

where r_0 is given by the following equation:

$$r_0 = \frac{e^2}{\varepsilon k_B T} \qquad 17$$

Thus the diffusion limited rate constant for reactions involving ions is,

$$k_D = \frac{-4\pi(D_A + D_B) z_A z_B r_0}{1-\exp(z_A z_B r_0 / R)} \qquad 18$$

The diffusion limited rate constant of neutral species in solution compared to ions under similar conditions is dependent upon the ratio of β/R. For a system where $z_A z_B = -1$, as is the case here, this ratio is on the order of 2-10, depending on molecular size, with rate constants for solutions containing oppositely charged ions being larger than those for the neutral species. This is expected considering the coulombic attraction of oppositely charged particles.

Of course, when comparing rates of reaction, especially the forward electron transfer rate and the backward electron transfer rate (not geminate recombination) it is especially important to consider the concentration of the species involved. The concentration of the neutral species is, in many cases, significantly larger than that of the photo-induced ions.

Other solvent and solute specific parameters, such as charge state stability, orientation constraints, spin considerations and side reactions can affect the rates and the concentrations of species converted. Competing pathways such as radiative and non-radiative relaxation of excited species and back electron transfer diminish the overall yield of the charged species that are to be used in optical limiting. Therefore, in order to understand and maximize the production of the charged species, the quantum efficiency of a photo-induced reaction can be determined. Measurement of the quantum efficiency of the reaction under various experimental conditions such as different solvents, concentrations and donor/ acceptor combinations gives information which will allow improvement in the efficiency of the charge transfer state formation and rational design of optical limiters.

Statement of Problem

History

The first class of compounds studied by the L.Spangler group as possible photo-induced absorbers and optical limiters was the bis-(diphenylamino) diphenylpolyene series depicted in Figure 5. The compounds posses many of the qualities that make them interesting for limiters study. Their ground state absorption in the visible is minimal, especially for the compounds with fewer double bonds, as they appear virtually colorless to orange. This allows for good visibility and color perception in a practical device. They are known to form chemically stable bipolaron states that have broad, intense absorptions. The possibility of polaron states exists as well, although they had not been chemically generated because it was thought that they would be unstable in solution. It remained to be seen, however, if the ionic states could be generated using light.

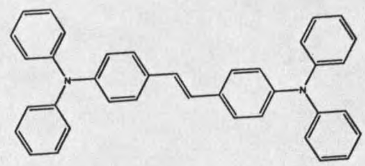

n=1

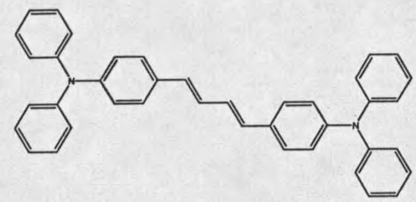

n=2

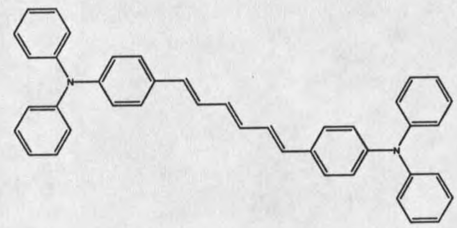

n=3

Figure 5. Oligimers n=1, n=2 and n=3 of the Bis-(diphenylamino) diphenylpolyene Series.

The molecule designated n=3 (due to the three double bonds in the polyene backbone) was the first to be tested. It was put in to o-dichlorobenzene with C_{60}, a known electron acceptor[7], in a 1:1 ratio. Upon excitation with 514nm and 488nm laser light from a CW Argon ion laser, three distinct PIA peaks were seen in the 15000 cm^{-1} to 10000 cm^{-1} region. The peaks were only present when the donor and acceptor were in solution together, indicating a cooperative effect. The identity of the peaks was at first uncertain; they did not display the broad, featureless absorption of the bipolaron and the λ_{max} was at the wrong wavelength for this species and the initial search for a corresponding anion or di-anion absorption was also fruitless.

An attempt to chemically generate the polaron of the bis-(diphenylamino) diphenylpolyene series was undertaken. A significantly diluted (1x 10^{-4}M) solution of antimony pentachloride was added dropwise to a solution containing the chromophore and spectra were taken after each addition of oxidizer. The resulting absorption spectrum was similar to that seen in the PIA spectra indicating the formation of a polaron in the photo induced experiment. Lower time resolved PIA spectra were taken of the donor-acceptor systems in the NIR region and the better signal to noise ratio afforded by these data allowed for positive identification of the C_{60}^- peak at 9300 cm^{-1} [8] confirming photoinduced charge transfer (PI-CT) in these systems.

The diphenylamine and polyene backbone moieties incorporated into these molecules were used in an attempt to enhance their non-linear capabilities. The extended pi-system promotes conjugation along the molecule's backbone which makes the molecule highly polarizable, an ideal trait for non-linear applications. In fact, the molecules are good two-photon absorbers. The conjugation permits delocalization and possibly stabilizes the cation and the dication formation. There is still some debate as to whether the charge remains localized on the nitrogen or if it is dispersed through the system. It was also speculated that a dendrimer based on these model chromophores would have enhanced capabilities due to the possibility of two dimensional conjugation.

Current Molecules

Two dendrimers based on the n=1 oligimer were synthesized (see Figure 6). which are designated the 3 arm and 4 arm n=1 dendrimers. Studies of the three arm dendrimer are discussed in Wendi Sonnenberg's thesis[9]. The PIA studies of the four arm dendrimer including rates of solvated charged state formation and charge recombination, will be presented here.

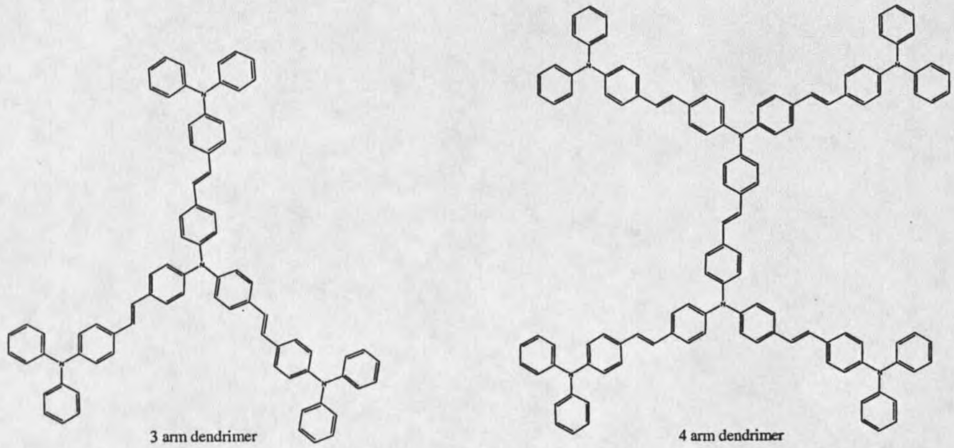

Figure 6. 3 arm and 4 arm n=1 Dendrimers.

The ultimate goal of this project is to create an optical limiting device. Ideally, such a material will be in a solid state form such as a polymer or gel or coated on to a solid substrate. Incorporation into a polymer backbone and easy dendrimer synthesis are desirable as one can control such parameters as the distance between donor and acceptor molecules as well as concentration of the chromophores. To this end, a new group of compounds with similar structural moieties to the original bis-(diphenylamino) diphenylpolyene series was synthesized by Kimba Ashworth in Dr. Charles Spangler's group[10]. These structures are pictured in Figure 7. They are very similar to the original series, however they have been modified with a hydroxy linkage to facilitate their addition into a polymer host as well as their formation into dendrons and dendrimers. The analysis of the PI-CT capabilities of this new group of materials will be investigated including a look at the solvated charge formation and charge recombination rates of these compounds as well as a comparison between the charge transfer efficiency of the n=3 oligimer, dendron and dendrimer of this series as analyzed by the isobestic point method. A discussion of the original mechanism proposed and the modifications made necessary by quantum efficiency measurements is also a primary conclusion.

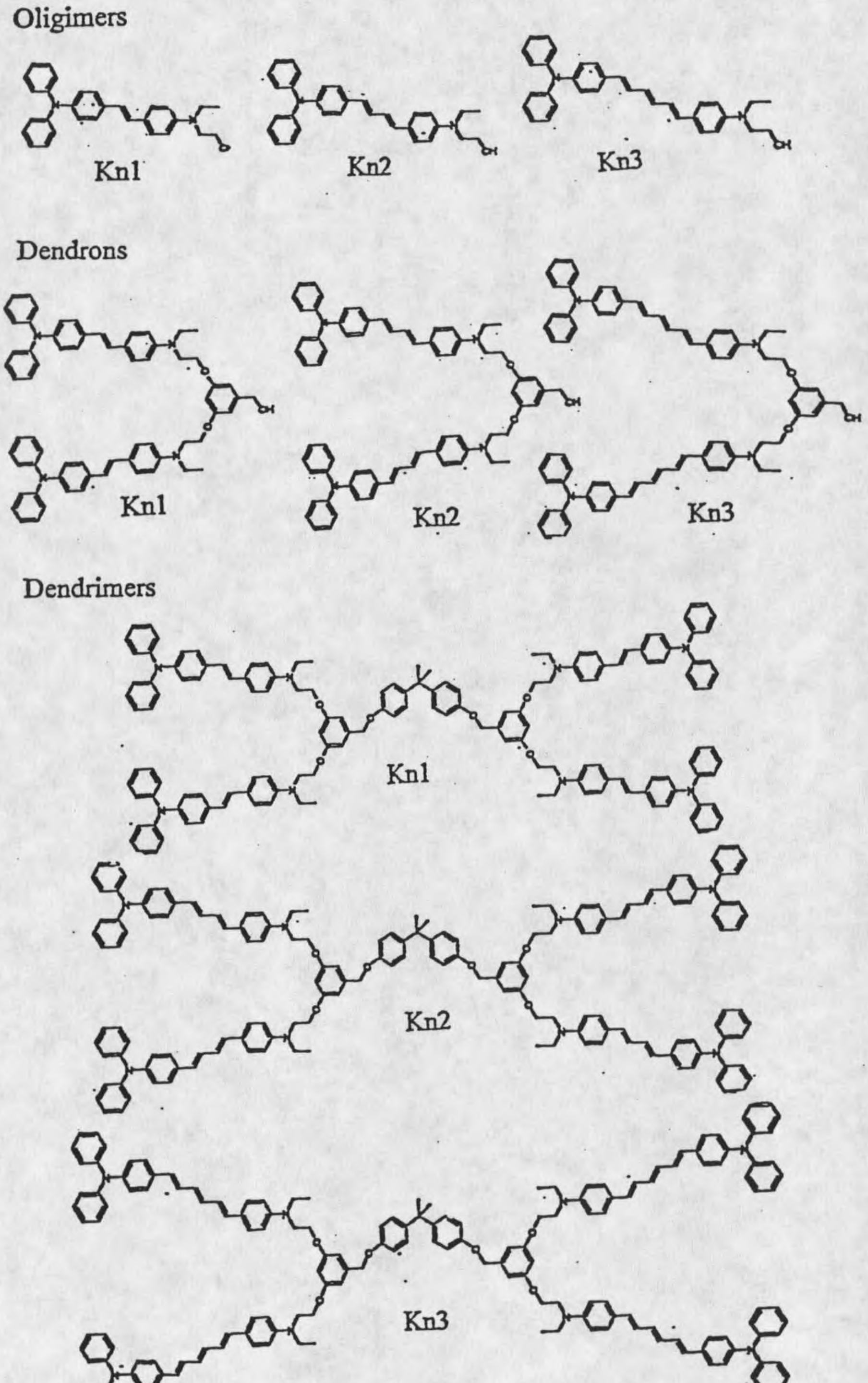

Figure 7. Hydroxy Substituted diphenylamino diphenylpolyenes Series. Kn1, Kn2 and Kn3 oligimers, dendrons and dendrimers

CHAPTER 2

FOURIER TRANSFORM SPECTROSCOPY

General

Fourier Transform Infrared (FTIR) and visible (FTVIS) spectroscopy have been used for many years as a trusted analytical tool. FTIR is especially prevalent in the identification of organic molecules through their characteristic absorptions in the "fingerprint region" of the mid-IR spectral region. Recently, Fourier Transform interferometry has become a very powerful tool in the analysis of time-resolved phenomena such as the dynamics of laser materials and, as will be shown here, transient absorption.

The FT instruments used in this study utilize a Michelson interferometer (Figure 8). The interferometer consists of two mirrors, one that is held stationary, M1, and one that can be moved, M2, and a beamsplitter, BS. Light enters the interferometer and is divided into two paths by the beamsplitter. Half of this light is reflected to the stationary mirror and half passes through to the moving mirror. The light is then reflected back along the same path by the respective mirrors and recombines at the beamsplitter where half of this light is transmitted and half is reflected. It is the transmitted light from the stationary mirror and the reflected light from the moving mirror that passes on to the detector. When the light from the two mirrors, M1 and M2, recombines at the beamsplitter, it will interfere, providing a means of wavelength discrimination. The nature of the interference, that is constructive or destructive, depends on the relative pathlength difference that the light has traveled. The easiest way to picture this is to imagine a single frequency of light passing through the interferometer. If the stationary mirror is at a distance x from the beamsplitter, then the light will constructively interfere when the moving mirror is at a distance $(n * \lambda/2) + x$, ($n * \lambda$ total path length difference) from the beamsplitter, where n is an integer and λ is the wavelength of light. When the moving mirror is $(n * \lambda/4) + x$ ($n * \lambda/2$ total path length difference) from the beamsplitter, there is destructive interference. As the moving mirror is translated, the single frequency will oscillate between total constructive and total destructive interference. A plot of the intensity change versus mirror position (the mirror position can be converted to time using the path difference and the speed of light), known as an interferogram, yields a sine wave. The Fourier transform of this sine wave gives a delta function at the frequency of the light used.

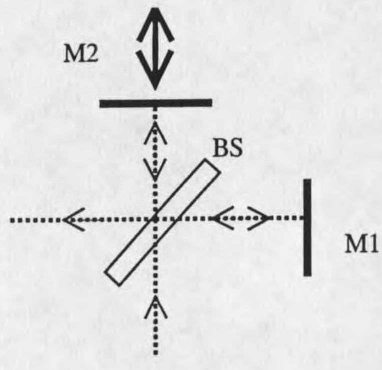

Figure 8. Michelson Interferometer. M1: Stationary mirror; M2: Moving mirror; BS: Beamsplitter; dashed line: light path.

If white light is passed through the interferometer, the different wavelengths of light will have differing levels of interference at each mirror position. Therefore, a more complex interfereogram is obtained. Nonetheless, a Fourier transform of this data will give the original frequencies and their intensities. It is the ability to differentiate between light frequencies while simultaneously transmitting these wavelengths, known as the multiplex advantage, that is an attractive feature of FT instruments.

Operating Modes

Typically, the interferometer is operated in continuous scan mode. In this case, the moving mirror is cycled through the necessary path length at a constant velocity. The position of the moving mirror is determined by using the interference pattern of a reference laser (in this case, a Helium Neon, HeNe, laser at 632.8 nm). Data is collected at every "zero crossing" or every time the sine wave value is zero. Continuous scan operation is generally used to take absorption or CW emission spectra.

The interferometer can also be used in step scan mode in order to take time resolved spectra (Figure 9). In this case, the interferometer is used in conjunction with a modulated or pulsed source, such as a pulsed laser. The moving mirror is stepped to a certain position and held there as the detector signal is digitized at multiple points in time using a transient digitizer. The temporal resolution can be set by the user and is currently limited by the response time of the detector and the speed of the electronics. The typical limit of resolution in the L. Spangler lab is 25-50ns. The mirror is then moved

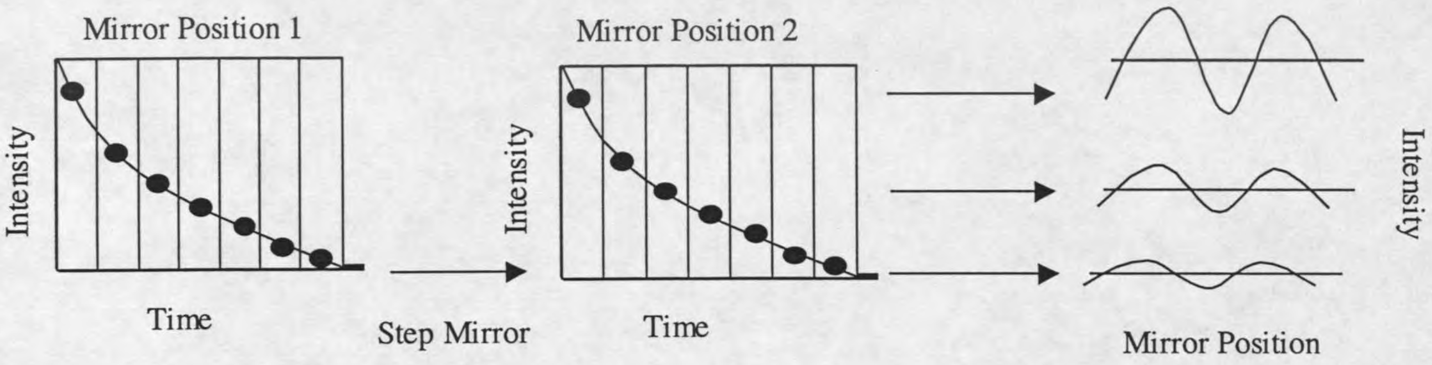

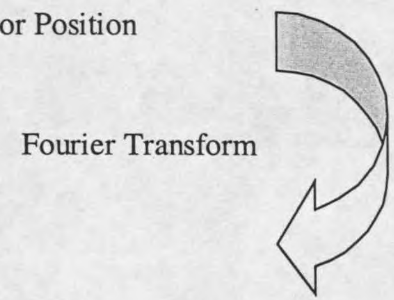

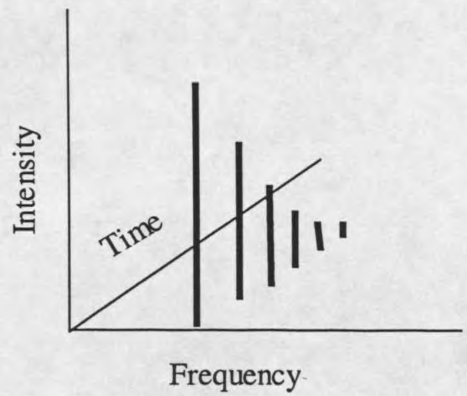

Figure 9 Step Scan Fourier Transform Interferometry. Assume that a single time dependant frequency is being detected. The signal will be digitized at several different time slices (small rectangles) at each mirror position (large blocks). The mirror is then stepped to a new position and the process repeated. The data points in each time slice for each mirror position are then combined to form the interferogram . These interferograms are then Fourier Transformed to yield a time and frequency resolved spectrum of the signal.

to a new position and time dependant data is collected again. In order to get better signal to noise, data acquisition at each mirror position can be repeated and the values averaged, referred to as co-additions. Step scan mode generates a three dimensional array of data consisting of time, mirror position and intensity. If the intensity reading at each mirror position for one time slice is compiled, a interfereogram at that time is generated. This can then be repeated for each time slice and these interferograms are then Fourier transformed to generate a time and frequency resolved spectra.

Measuring PIA with FT Interferometry

Fourier transform spectroscopy (FTS) was applied by the L. Spangler group to measure PIA spectra. Typically, PIA spectra are measured using dispersive instruments, the main disadvantage of which is the time required to gather complete time and frequency resolved data. In order to gather time resolved data with fine temporal resolution, a monochromator must sacrifice either wavelength resolution or spectral range, as it cannot scan a high spectral resolution spectrum across many wavelengths in a short period of time. Therefore, temporal traces are often gathered at one wavelength at a time. A large spectral region can therefore take a significant period to sample, especially at high resolution. In contrast, a relatively high resolution (100 cm^{-1}, 50ns) data set takes approximately 20 minutes or less with good signal to noise using step-scan FT methods.

A major disadvantage to using an interferometer for taking step-scan data is the current inability to collect spectral data on both sides of the HeNe reference laser at one time. This limitation is due to electronics involved in data acquisition. This means that spectral information near the HeNe wavelength is difficult to obtain, due to the cut-off filters that must be used to prevent "folding". Folding or aliasing is a problem that plagues Fourier transform instruments if the spectral region that is to be treated is smaller than the region that the detector can detect. Figure 10 explains the process pictorially.

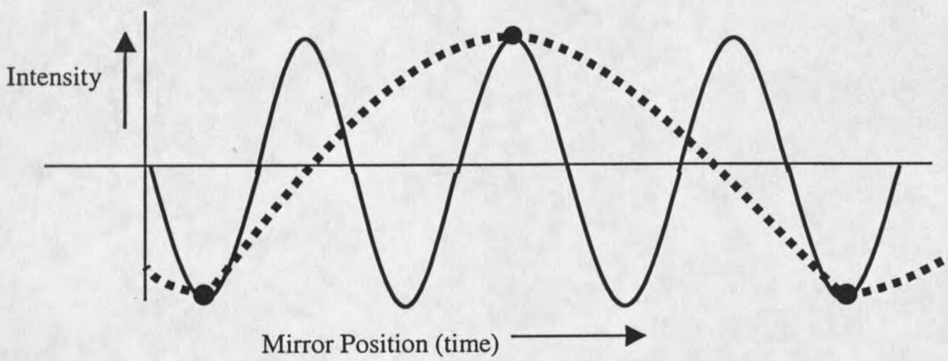

Figure 10. Pictorial Description of Aliasing. Points represent positions of data digitization. The solid line is actual frequency and the dashed line is aliased frequency .

The points that are digitized by the detector in Figure 10 are actually due to the frequency designated by the solid line. This frequency can be detected by the system, but is outside of the region to be Fourier transformed. The frequency designated by the dashed line also fits these points and is in the frequency range covered by the FT. This frequency will therefore appear in the resulting spectrum, even though it does not actually exist. In order to prevent this effect from entering into spectra, it is necessary to block all light outside of the Fourier transform region. The problem of not being able to cross the HeNe in step scan mode is currently being addressed by the L. Spangler group.

Three methods for characterizing PIA using FTS are being used. All involve the same experimental geometry illustrated in Figure 11. White light from a quartz tungsten halogen bulb passes through the sample and then into the interferometer. A laser beam is directed though the same sample volume in a quasi co-linear alignment. This laser is either CW, modulated or pulsed, depending on the experiment. The signal from the interferometer can be treated in a variety of ways as will be described.

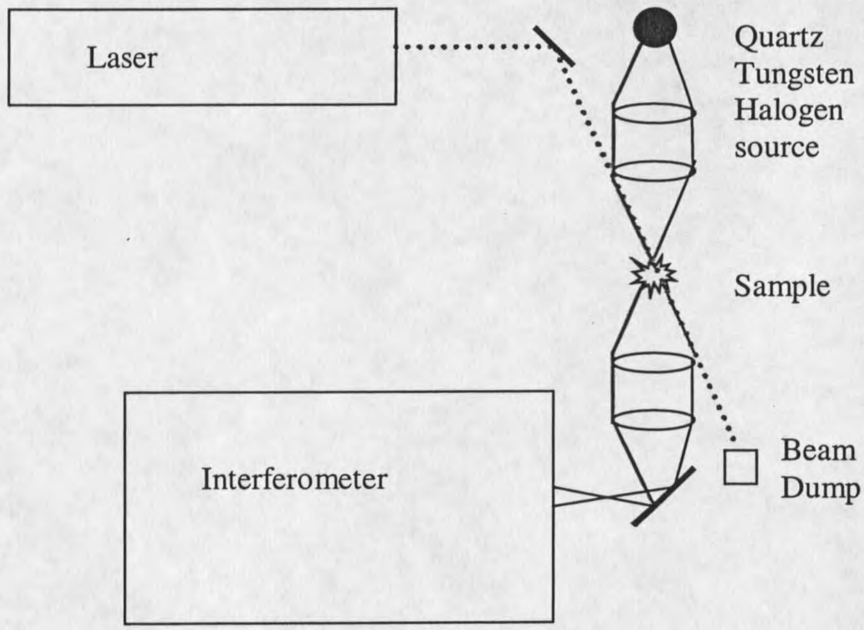

Figure 11. Basic Geometry for FT-PIA Experiments. The QTH bulb is the probe source and the laser is the pump source. The laser can be CW, mechanically modulated or pulsed.

Difference Method

The most simple PIA experiment involves taking sufficiently accurate absorption spectra of the sample with a CW (or effectively CW) laser incident upon the sample as well as with the laser off. The difference between these two spectra is divided by the ground state absorption, or unpumped, spectrum to generate the PIA curve. This data is not time resolved and merely gives wavelength and steady–state intensity information. The sensitivity of the measurement depends upon the signal to noise of the individual spectra taken.

Modulated Method

The second method involves a conceptually different way at obtaining difference spectra. Phase-sensitive detection is used in this case, which is usually more sensitive to small changes in intensity. The laser is modulated using a mechanical chopper. The detector signal from the interferometer is then fed into a lock-in amplifier, which is synchronized to the reference signal provided by the chopper and only amplifies signals that modulate at the same frequency as the laser pulse. There are two signals that occur at this frequency: laser induced emission and laser induced changes in the absorption of the white light. Emission and photo-induced transparency are easily distinguished from PIA based on their phase relationship to the laser pulse. The signal that comes out of the lock-in amplifier is therefore the difference between the absorption of the material with the laser on and with the laser off. This signal is fed back into the interferometer which is being operated in step scan mode. At each mirror position, a data point (or several if averaging is desired) is taken after a user defined delay time which is adjusted to account for the time constant of the lock-in. The data points are then compiled into an interferogram and the resulting spectrum is divided by a spectrum of the sample's ground state absorption. Careful consideration must be placed on the differences in gain settings used to collect these two spectra if accurate intensity values are to be generated. This data is not time resolved and the acquisition tends to favor longer lived species as the lock-in amplifier effectively integrates the peaks in time. This method is good at providing the position of peaks with high sensitivity.

Time Resolved Method

The most informative method of data collection is time resolved PIA using the step scan FT instrument which has been described above. A pulsed laser is used as the pump source to create the transient species and the signal that is digitized is the white light probe which yields broadband absorption information. Several time traces are taken before the laser hits the sample, which provide ground state absorption information about the sample. All of the time resolved traces are subtracted from the average of the traces taken before the pump (unpumped traces) to give the absorption difference. In order to correct for the instrument and filter response, as is typically done, the difference spectra are then divided by the average unpumped trace to give $\Delta T/T$. The result is the temporal behavior of the absorption of the transient species created when the laser pulse encounters the sample. Because the spectra are fully time and frequency resolved, it is possible to watch the transfer of population from one species to another and to identify possible intermediates that may not have been so easily spotted using other methods as well as extract valuable kinetic data and quantum efficiencies.

CHAPTER 3

EXPERIMENTAL PROCEDURE

Sample Materials

Purified donor samples were obtained from Dr. Charles Spangler's research group at Montana State University. All samples were powders and ranged in color from bright yellow to orange-red. C_{60} was obtained from Texas Fullerenes Corporation at 99% purity. Solutions were made using o-dichlorobenzene (ODCB), 99.9 % or CH_2Cl_2, HPLC grade from Fisher Chemical Company as solvent. The concentrations of each donor/acceptor solution tested are listed in Table 1.

Compound	Concentration	Compound	Concentration
KN1 oligimer/C_{60}	0.5mM/0.5mM	KN2 dendrimer/C_{60}	0.5mM/0.5mM
KN1 dendron/C_{60}	0.5mM/0.5mM	KN3 oligimer/C_{60}	0.5mM/0.5mM
KN1 dendrimer/C_{60}	0.5mM/0.5mM	KN3 dendron/C_{60}	0.5mM/0.5mM
KN2 oligimer/C_{60}	0.5mM/0.5mM	KN3 dendrimer/C_{60}	0.5mM/0.5mM
KN2 dendron/C_{60}	0.5mM/0.5mM	4arm dendrimer/C_{60}	0.1mM/0.1mM, 0.25mM/0.25 mM, 0.5mM/0.5mM, 1.0mM/0. 5mM

Table 1. Compounds and Concentrations Studied

Instrumental

Approximately 2mL of the solutions was placed in quartz or glass cuvettes with 1 cm path length obtained from Starna Cells Inc. The cells were cleaned using either a base or acid bath with a distilled water rinse. The outside of the cells was cleaned with either HPLC grade acetone or methanol. Nitrogen gas was bubbled through the samples for approximately twenty minutes before PIA testing to de-oxygenate and then sealed with Teflon caps and Parafilm.

Absorption spectra of the chromophore alone, bipolaron and the chromophore with C_{60} were taken on a Bruker IFS88 interferometer and a Shimadzu 3101PS UV/VIS instrument which had better performance in the UV and blue spectral regions. The solvent, CH_2Cl_2 for chromophore alone and bipolaron and ODCB for donor acceptor systems, was used for the background.

Spectra of chemically oxidized polarons were collected using the Bruker IFS 88. The quartz beamsplitter and silicon diode detector were used, as the region of interest extended from 25000 cm^{-1} to 10000 cm^{-1} . 2 mL of a solution of the chromophore at 1×10^{-5}M in CH_2Cl_2 was placed in an open cuvette which was gently stirred to encourage thorough mixing, yet not disturb the light passing through the sample. A solution of 2×10^{-4} M $SbCl_5$ in CH_2Cl_2 was added dropwise to the cuvette via a 1 cc syringe and a fine gauge needle. A spectrum was taken after each addition of oxidizer (usually 5-10 drops at a time) until 2mL of the $SbCl_5$ had been added. These spectra were divided by the ground state absorption spectrum of the neutral chromophore.

Difference and modulated PIA measurements used the Bruker IFS 88 interferometer and a Coherent Sabre Argon ion laser to pump the samples at 488nm and 514nm. The beam was turned using right angle prisms and the full beam waist of approximately 5mm was used. The power of the beam was adjusted to 200-250mW by controlling the current supplied to the Ar^+ tube. In the case of the modulated experiments, a PTI OC4000 mechanical chopper was used with a modulation range of 1-1000 Hz. The white light probe was a quartz tungsten halogen bulb encased in a water cooled jacket. This housing was placed inside of a wooden box with a one inch diameter aperture in order to further stabilize the lamp temperature. The light was focused through the sample with a long focal length so that the diameter of the probe beam did not change too much through the cuvette. It was then collimated and re-focused with lenses appropriate for matching the interferometer's F/4.5 optical system. An adjustable iris was placed at the external focal point of the interferometer so that the light could be attenuated to prevent saturating the detectors and electronics. Filters to cut stray laser light were placed in the sample chamber. The Si/quartz detector/beam splitter combination was again used. A model SR510 lock-in amplifier from Stanford Research Systems was used for the modulated method with an AC-coupled detector. Spectra were taken with the laser off and with the laser on in the case of the difference method or with the laser on while being chopped in the case of the modulated method, which were then treated to yield the PIA of the sample.

Time resolved PIA spectra were taken using the Bruker IFS 66 interferometer. The pump source was the doubled output (532nm) of a Coherent Infinity 40-100

Nd:YAG laser operating at 50 Hz. The pulse is TEM_{00} and has a length of approximately ~7ns. In order to maintain stability of the laser and reduce pulse to pulse fluctuations to a standard deviation of ~1%, the laser was operated at a voltage sufficient to produce 250mJ of the fundamental (1064nm) or higher. The beam was directed using 532nm dichroic mirrors which passed the fundamental 1064nm beam that runs co-linearly with the 532nm, acting as a effective filter. The beam was split by a 70-30 beamsplitter and the beam of lower magnitude was then directed through a CaF_2 Glan-Laser polarizer and a filter to control the attenuation of the beam and therefore the power. The polarizer was adjusted so that the average energy of one pulse was 1.2 mJ. In order to control the diameter of the beam, a fixed aperture was placed in the path just before the laser encountered the sample. Filters, consisting most often of a red pass filter and an additional filter designed to block as much of the laser light as possible, were placed in the internal sample chamber of the interferometer. The silicon diode detector and quartz beam splitter were used for the 25000 cm^{-1} to 10000 cm^{-1} spectral region. A liquid nitrogen cooled InSb detector and a CaF_2 beam splitter were used for the 16,000 cm^{-1} to 2000 cm^{-1} region. Two temporal regimes were examined and each required the use of fast pre-amplifiers with the detectors. Data taken at 5 μsec time resolution used the internal analog to digital converter (IADC) while that taken at 50 nsec resolution required the PAD32 board, which has faster time response than the IADC.

All data was acquired using OPUS 3.1 which is the software that is included with the interferometers. Time resolved data was acquired with 200cm^{-1} spectral resolution and either 101 time slices at 5 μsec or 401 time slices at 50 nsec temporal resolution with

80 co-additions. Optical density calculations and optical density versus time traces were generated using OPUS and the exponential and linear fits to the data were performed using Microcal Origin version 4.10.

CHAPTER 4

RESULTS AND DISCUSSION

Basic Absorption Measurements

Initially, absorption spectra were taken of the various compounds tested (Figures 12-15)[10] as well as the compounds in solution with C_{60} (Figures 16-19). Each of the donor molecules has minimal absorption in the visible which is ideal for optical limiting applications. The acceptor, C_{60}, does have absorption in the visible region, however, it is possible to reduce this to a more desirable transmittance level by adjusting the concentration as long as efficiency is not compromised. The absorption at 532nm , given in Table 2, was of primary concern as this is where the molecules were to be excited. It was determined that C_{60} is the primary absorber at this wavelength for the Kn1, Kn2 and the 4 arm dendrimer solutions. Kn3 absorbs a small amount at 532nm, which was evidenced both by the absorption spectrum and by the presence of laser induced emission. Importantly, the ground state absorption of the donor and acceptor together in solution revealed no appreciable ground state charge complex formation; the absorption spectrum is just the combination of the two species' absorptions were they alone in solution.

The polaron of the 4 arm dendrimer was the only species in this study to be chemically induced. This was mainly due to the availability of the compound, as there was a minimal amount of the hydroxy series with which to work. New solutions at 0.01mM were made because chemical oxidation required the use of methylene chloride as a solvent because $SbCl_5$ will oxidize the benzene ring in ODCB. The chemically oxidized absorption spectrum of the 4arm dendrimer exhibits peaks very similar to those seen in the chemically and photoinduced spectrum of the original bis-(diphenylamino) diphenylpolyene oligimer with one double bond (n=1) seen in Figure 5. This is expected as it is the parent molecule of the dendrimer. The visible peak is broad and fairly featureless (Figure 20), although on close examination it does display small bumps which bear resemblance to the two or three more distinct peaks of the polarons of the molecules in the same series with longer conjugation lengths. The detectable IR peaks in this series have a strong absorption cross section and are gaussian type bands. The peak in the IR region for the 4 arm dendrimer is significantly more red shifted than the IR peak of n=1 oligimer. This absorption may be due to a intervalence transition between the ground state potential well of the polaron and a potential well created by the avoided crossing of the different minima present in the molecule[11,12,13,14], presumably located at the nitrogens (Figure 21). It is clear that the dendrimer behaves in a qualitatively similar fashion to the n=1 oligimer in the visible region of the spectrum, where the development of optical limiters is currently focused.

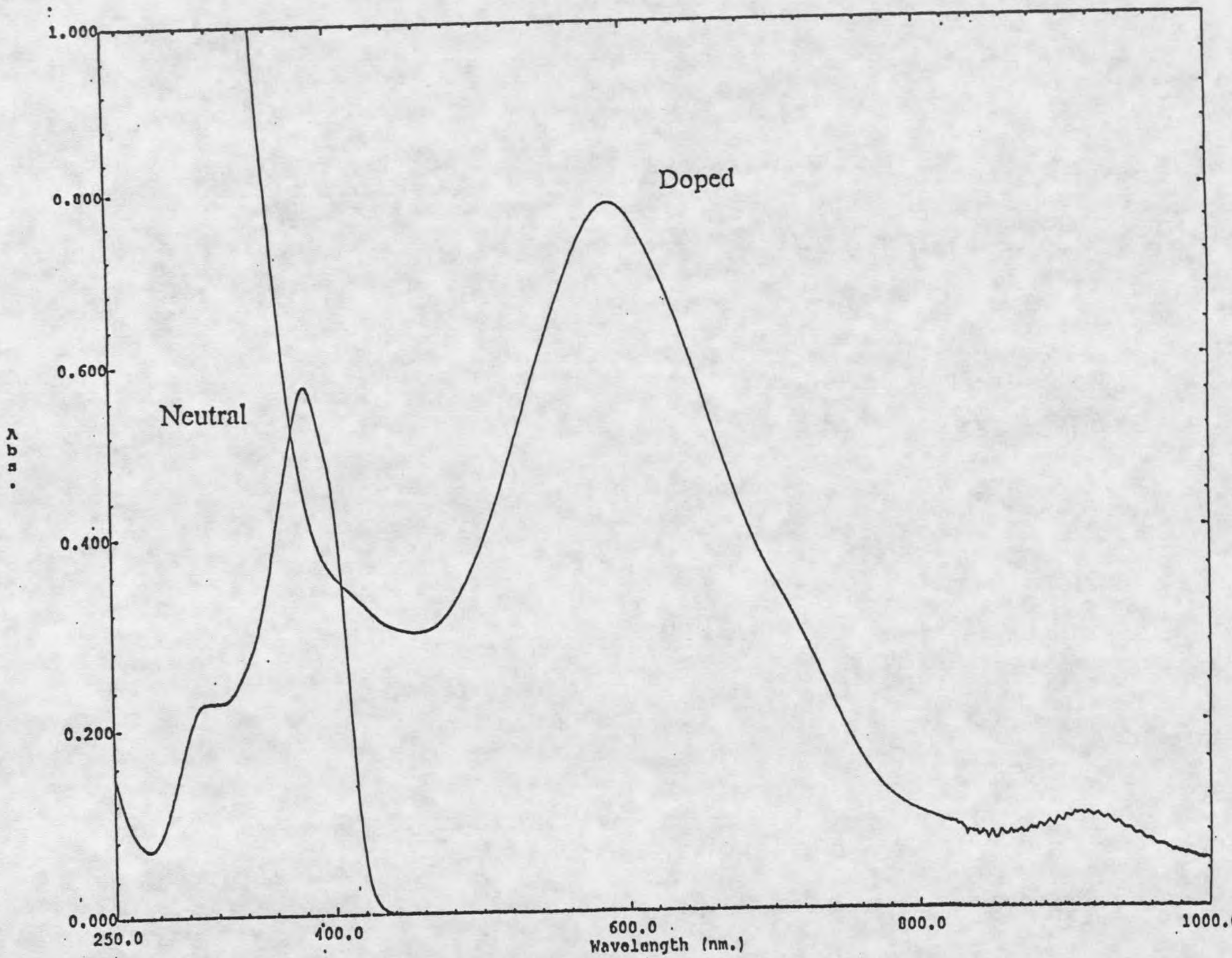

Figure 12. Absorption Spectra for Neutral and Bipolaron (Doped) Kn1 Chromophore

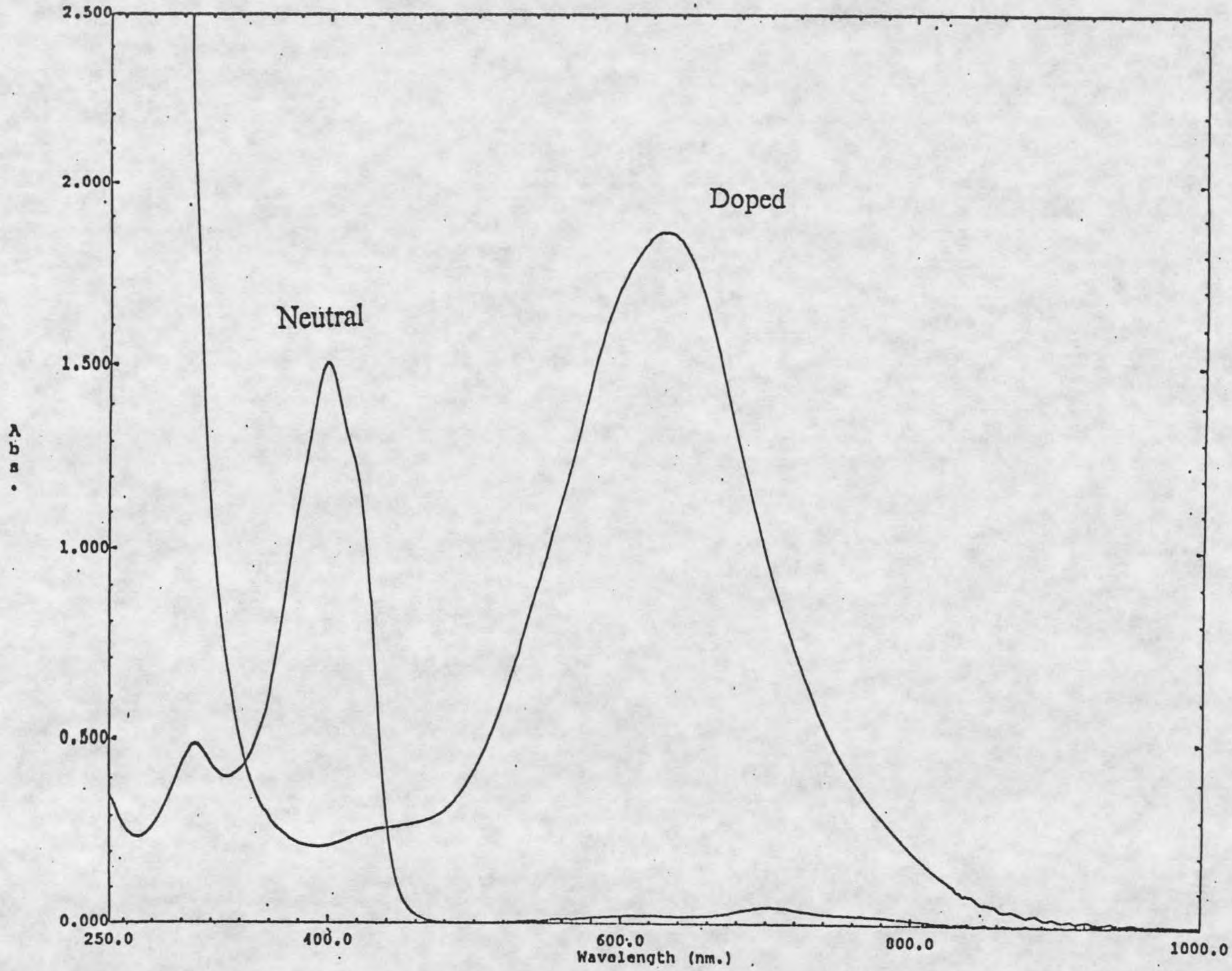

Figure 13. Absorption Spectra for Neutral and Bipolaron (Doped) Kn2 Chromophore

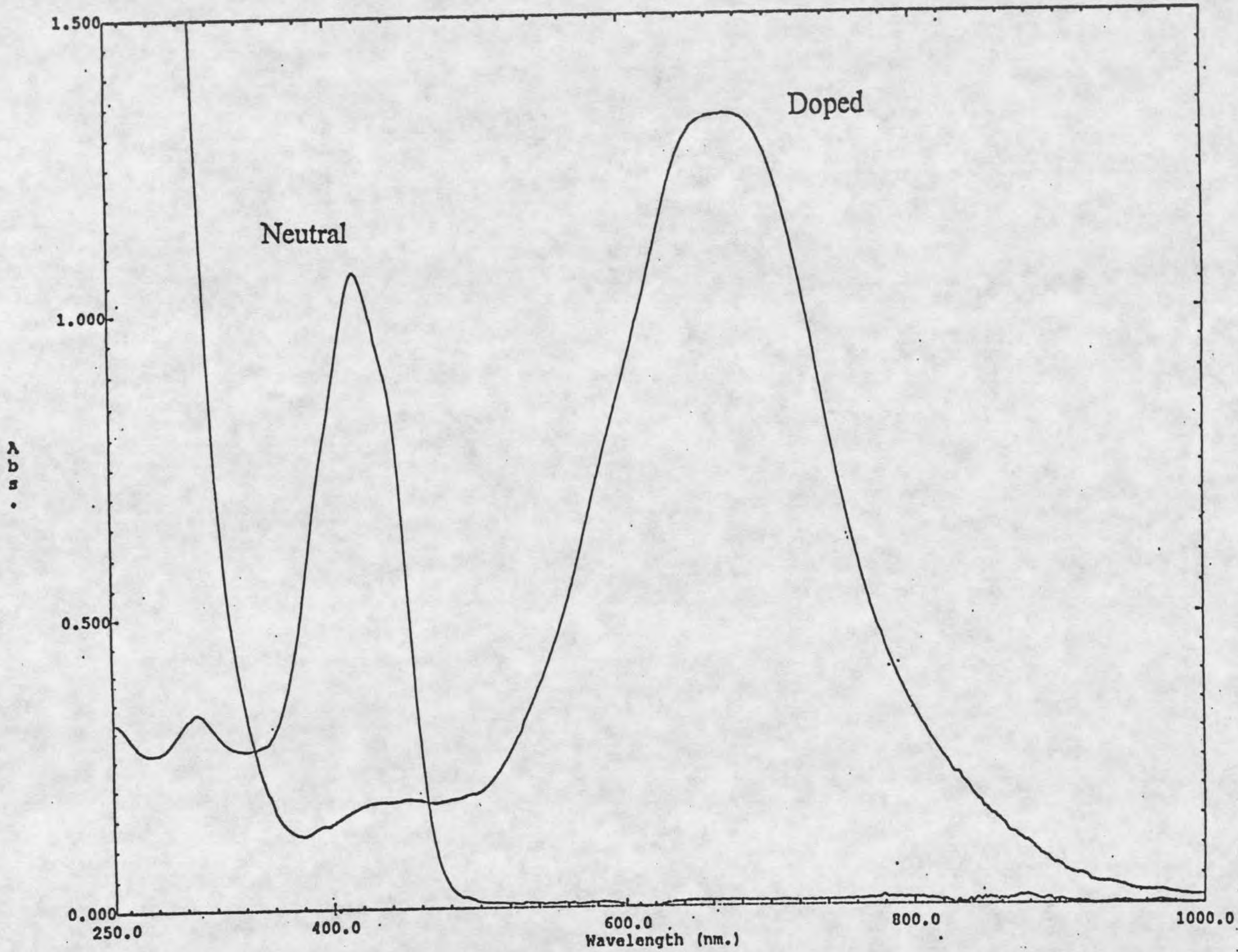

Figure 14. Absorption Spectra for Neutral and Bipolaron (Doped) Kn3 Chromophore

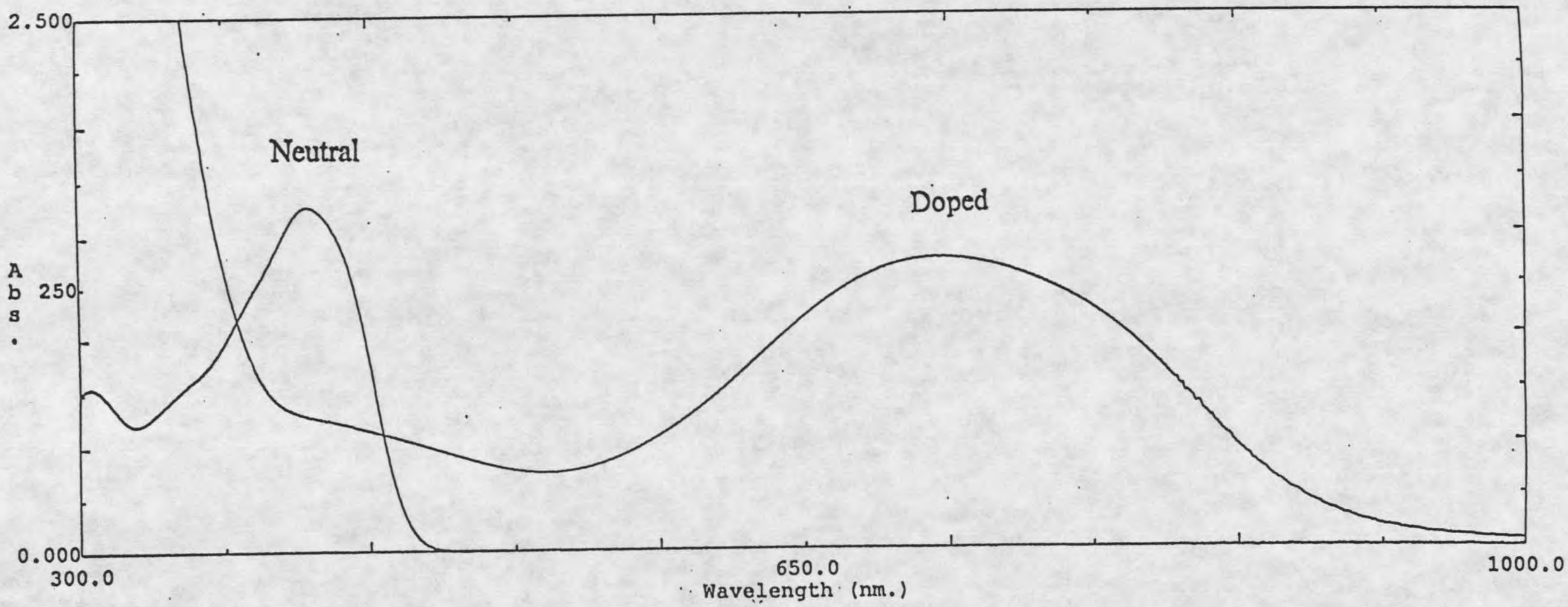

Figure 15. Absorption Spectra for Neutral and Bipolaron (Doped) 4 arm Dendrimer.

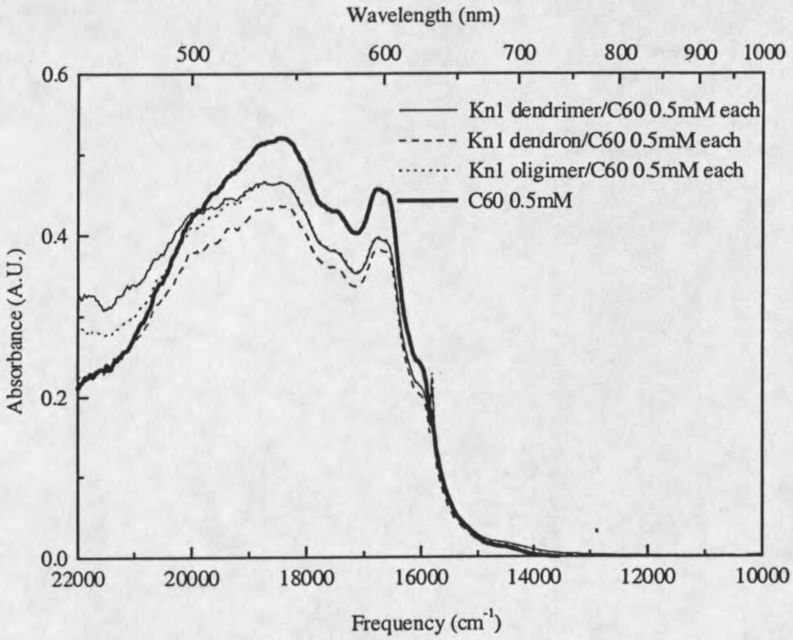

Figure 16. Kn1 series with C_{60} Absorption compared to Absorption of C_{60} Alone.

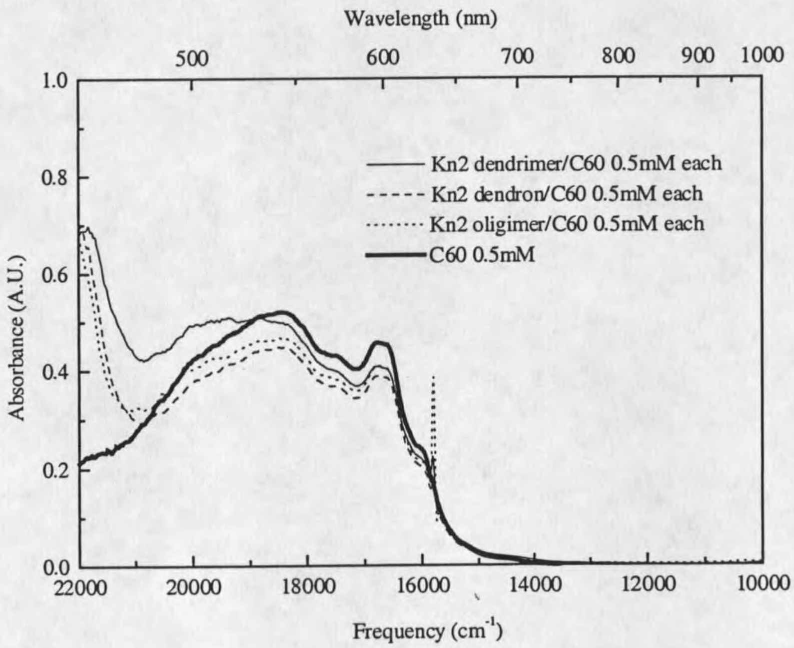

Figure 17. Kn2 Series with C_{60} Absorption Compared to Absorption of C_{60} Alone.

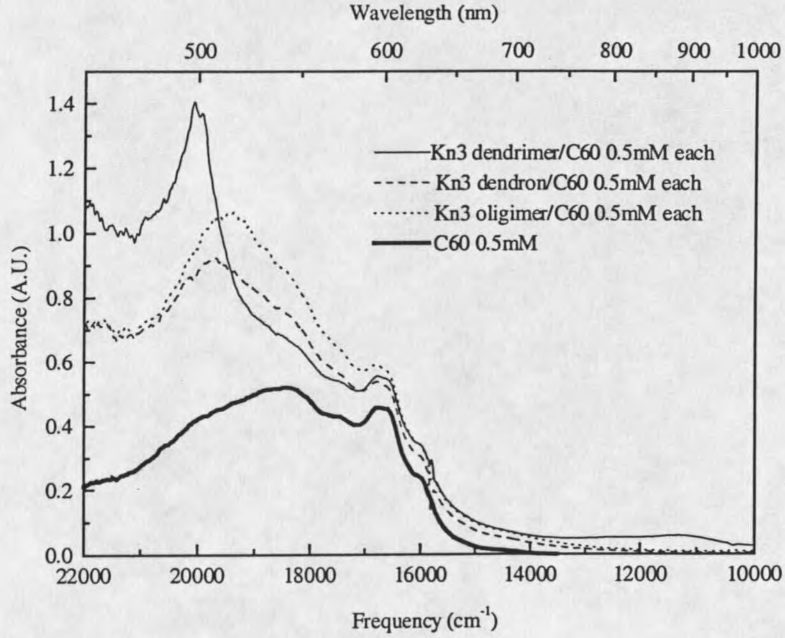

Figure 18. Kn3 Series with C_{60} Absorption Compared to Absorption of C_{60} Alone.

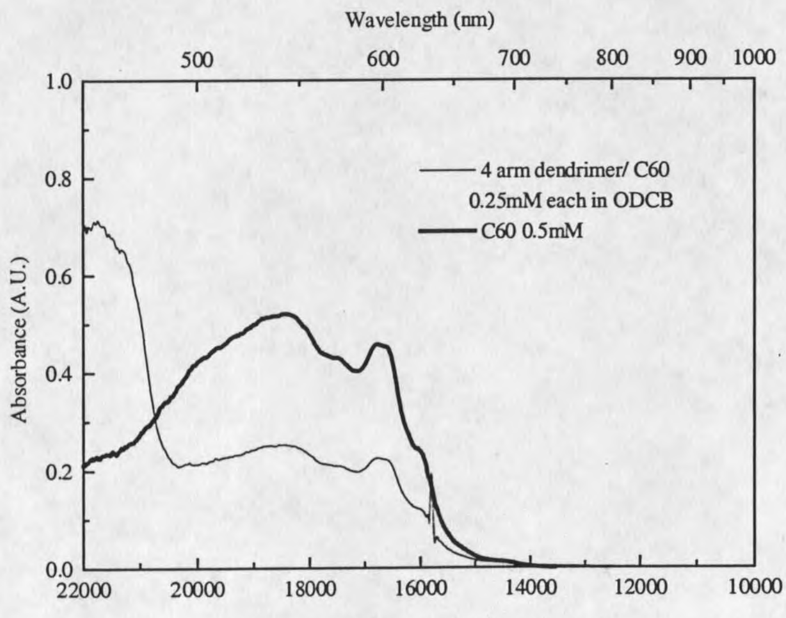

Figure 19. 4 arm Dendrimer with C_{60} Absorption Compared to Absorption of C_{60} Alone.